







Covalency does not suppress O₂ formation in 4d and 5d Li-rich O-redox cathodes

Robert A. House ^{1,2,3}, John-Joseph Marie^{1,2,3}, Joohyuk Park^{1,2,3}, Gregory J. Rees ^{1,2,3}, Stefano Agrestini⁴, Abhishek Nag ⁴, Mirian Garcia-Fernandez ⁴, Ke-Jin Zhou ⁴ & Peter G. Bruce ^{1,2,3}✉

Layered Li-rich transition metal oxides undergo O-redox, involving the oxidation of the O²⁻ ions charge compensated by extraction of Li⁺ ions. Recent results have shown that for 3d transition metal oxides the oxidized O²⁻ forms molecular O₂ trapped in the bulk particles. Other forms of oxidised O²⁻ such as O₂²⁻ or (O-O)ⁿ⁻ with long bonds have been proposed, based especially on work on 4 and 5d transition metal oxides, where TM-O bonding is more covalent. Here, we show, using high resolution RIXS that molecular O₂ is formed in the bulk particles on O²⁻ oxidation in the archetypal Li-rich ruthenates and iridate compounds, Li₂RuO₃, Li₂Ru_{0.5}Sn_{0.5}O₃ and Li₂Ir_{0.5}Sn_{0.5}O₃. The results indicate that O-redox occurs across 3, 4, and 5d transition metal oxides, forming O₂, i.e. the greater covalency of the 4d and 5d compounds still favours O₂. RIXS and XAS data for Li₂IrO₃ are consistent with a charge compensation mechanism associated primarily with Ir redox up to and beyond the 5+ oxidation state, with no evidence of O-O dimerization.

¹Department of Materials and Chemistry, University of Oxford, Oxford, UK. ²The Henry Royce Institute, Oxford, UK. ³The Faraday Institution, Quad One, Becquerel Avenue, Harwell Campus, Didcot, UK. ⁴Diamond Light Source, Harwell Campus, Didcot, UK. ✉email: peter.bruce@materials.ox.ac.uk

Layered Li-rich 3d transition metal oxide intercalation compounds, such as $\text{Li}[\text{Li}_{0.2}\text{Ni}_{0.13}\text{Co}_{0.13}\text{Mn}_{0.54}]\text{O}_2$, have received a great deal of attention because Li^+ can be extracted beyond the limit of transition metal (TM) oxidation, with the charge being compensated by oxidation of the O^{2-} ions (O-redox)^{1–9}. These compounds typically possess honeycomb ordered Li and TM within the TM layer. However, Mn-based honeycomb ordered structures do not provide a stable framework for oxidised O^{2-} and have been shown to undergo extensive TM migration, and bulk O–O dimerization leading to voltage hysteresis and loss of energy density, in addition to surface O_2 evolution^{10–14}. It has been shown recently that the dimerised O–O is molecular O_2 , which is trapped in voids within the bulk of the charged particles^{15,16}. Molecular O_2 formation is responsible for both surface O-loss and bulk O-redox.

Pioneering work by Tarascon, Doublet and co-workers^{17–25} and by others^{26–31}, on the 4d- and 5d-based analogues of the 3d compounds, such as Li_2RuO_3 , Na_2RuO_3 , $\text{Li}_2\text{Ru}_{0.5}\text{Mn}_{0.5}\text{O}_3$, Li_2IrO_3 and $\text{Li}_2\text{Ir}_{0.75}\text{Sn}_{0.25}\text{O}_3$, has led to important advances in the understanding of O-redox. These systems possess the same honeycomb ordered Li and TM ions within the TM layer. With the exception of Li_2IrO_3 , they exhibit voltage hysteresis, with a plateau on charge and a low voltage S-shaped profile on subsequent discharge. Loss of honeycomb ordering due to Li/TM disordering accompanies the voltage hysteresis along with O_2 loss from the surface of the particles^{17,19,21,26,29}. It has been reported that peroxides O_2^{2-} and longer O–O dimers form beyond the limits of transition metal oxidation in the 4 and 5d transition metal oxides^{17,19}. The more strongly hybridised TM–O bonding of the 4 and 5d transition metals compared with the 3d counterparts has been cited as a reason for stabilising such O–O species with longer O–O bonds^{18–20,32}. In highly covalent transition metal sulphides, selenides and tellurides, electron holes can be stabilised through dimerization of the chalcogen (S_2)²⁻ which remains coordinated to the transition metal due to the strong orbital overlap³³.

It has proved very challenging to identify experimentally the form of oxidised O^{2-} in charged materials. The recent application

of high resolution RIXS spectroscopy has proved useful in probing the nature of oxidised O^{2-} ^{15,16}. Here we apply this technique to the 4 and 5d materials, providing direct evidence for the presence of molecular O_2 , trapped in the bulk of the archetypal 4d and 5d systems Li_2RuO_3 , $\text{Li}_2\text{Ru}_{0.5}\text{Sn}_{0.5}\text{O}_3$ and $\text{Li}_2\text{Ir}_{0.5}\text{Sn}_{0.5}\text{O}_3$. The O_2 is formed only through charging across the high voltage plateau and is reduced on subsequent discharge, in line with our findings for $\text{Li}_{1.2}\text{Ni}_{0.13}\text{Co}_{0.13}\text{Mn}_{0.54}\text{O}_2$, disordered rocksalt $\text{Li}_2\text{MnO}_2\text{F}$ and the P2-type Na-ion cathodes^{15,16,34}. We find no evidence of molecular O_2 formation or other O–O dimers in Li_2IrO_3 up to the limits of oxidation and instead identify stable electron holes formed in bonding TM–O orbitals, consistent with previous reports indicating reversible Ir^{5+} to $\text{Ir}^{5.5+}$ oxidation instead of O oxidation and reinforcing the link between bulk O_2 formation and the loss of high voltage plateau²⁶. These data indicate that the more covalent TM–O bonding in 4 and 5d compared with 3d TM oxides still favours the formation of molecular O_2 , helping to explain why O-loss is also observed from the surface of these compounds. The implication is that the O-redox process, involving molecular O_2 formation at the surface and in the bulk, is the same for Li-rich systems with the honeycomb superstructure moving down the Periodic Table.

Results

The Li-rich ruthenates and iridates. Li_2RuO_3 , Li_2IrO_3 and Sn-substituted $\text{Li}_2\text{Ru}_{0.5}\text{Sn}_{0.5}\text{O}_3$ and $\text{Li}_2\text{Ir}_{0.5}\text{Sn}_{0.5}\text{O}_3$ were prepared following the methods of previous reports^{17,19}. Powder X-ray Diffraction data, Supplementary Figs. 1–3, confirm the formation of the compounds. Each of the materials possess O3-type layered structures with honeycomb ordering in the TM plane, Fig. 1a manifesting as the familiar superlattice peaks between $2\theta = 18^\circ$ and 34° . As seen before, there is evidence of some stacking faults between the ordered layers, which result in asymmetric peak broadening of these superlattice peaks, especially for the Sn-substituted samples.

The first cycle load curves are shown in Fig. 1b, c and are plotted against the nominal oxidation state of Ru and Ir

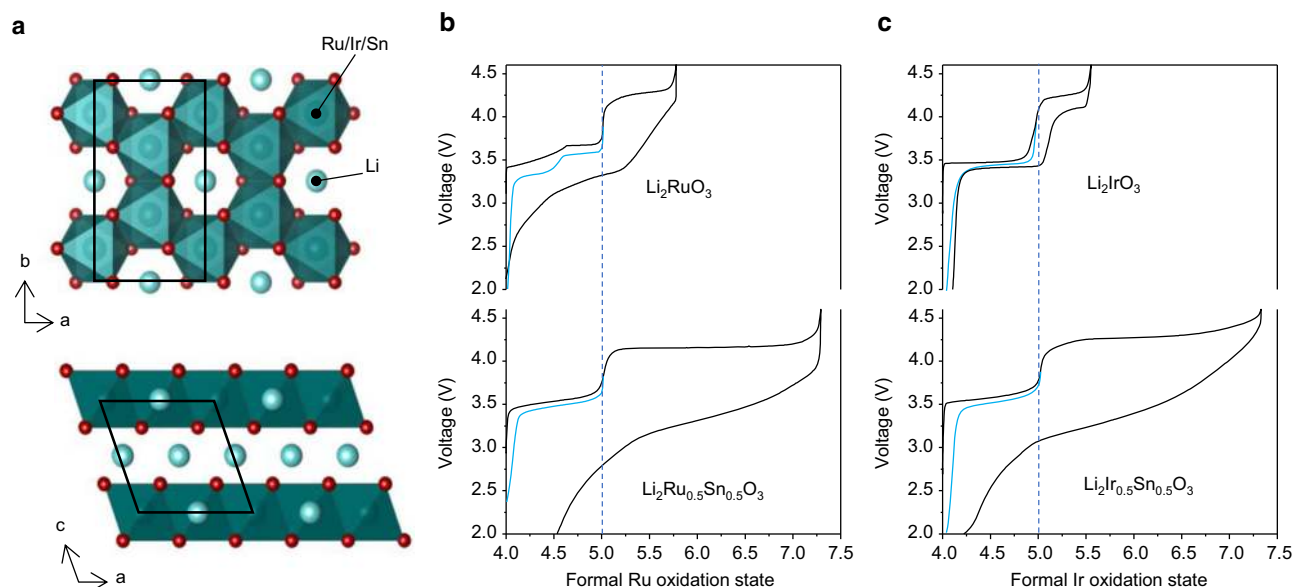


Fig. 1 Structure and electrochemistry of Li-rich 4d- and 5d-based cathodes. **a** O3-type layered structure with honeycomb ordering of Li and TM ions within the TM layers. First cycle load curves for **b** Li_2RuO_3 and $\text{Li}_2\text{Ru}_{0.5}\text{Sn}_{0.5}\text{O}_3$ and **(c)** Li_2IrO_3 and $\text{Li}_2\text{Ir}_{0.5}\text{Sn}_{0.5}\text{O}_3$ from 2.0 V to 4.6 V at a current rate of 20 mA g^{-1} plotted against formal oxidation state of Ru or Ir (in black). Electrochemical cycling is reversible with little voltage hysteresis below +5 (in blue). High voltage charging plateaus are observed in all materials beyond the +5 TM oxidation state. The plateaus are accompanied by significant voltage loss on subsequent discharge in all cases except for Li_2IrO_3 .

in each case, since Sn^{4+} is known to be redox inactive. The electrochemical behaviour is reversible with very little hysteresis when cycling below Ru^{5+} and Ir^{5+} . When sufficient Li is extracted to exceed the +5 oxidation state on Ru, an extended high voltage plateau is observed followed by an S-shaped discharge. For the iridates, reversibility can be maintained up to +5.5 supported by Ir redox as shown recently by Hong et al.²⁶ Further Li can be extracted beyond this limit in $\text{Li}_2\text{Ir}_{0.5}\text{Sn}_{0.5}\text{O}_3$ subsequently inducing voltage hysteresis. Li_2IrO_3 is the only material where TM migration and loss of the honeycomb ordering is avoided upon charging to 4.6 V, in accord with its reversible electrochemical behaviour^{26,30}.

Spectroscopic characterisation of O. Understanding O-redox has proven to be a challenge due in part to the need for techniques capable of determining the nature of O species formed in the bulk. In this study, we have employed X-ray absorption spectroscopy (XAS) in partial fluorescence yield (PFY) mode and high

resolution resonant inelastic X-ray scattering (RIXS) at the O K-edge, as they offer a direct probe of the electronic states on O at depths of up to 50–100 nm into the sample. XAS probes the empty states above the Fermi level. In RIXS, excitation of core electrons to empty states above the Fermi level results in emission as electrons from filled valance states below the Fermi level relax to the core-hole states. RIXS complements XAS as it provides a direct probe of the valance states on O.

In Fig. 2, we present the O K-edge XAS and RIXS for Li_2RuO_3 and $\text{Li}_2\text{Ru}_{0.5}\text{Sn}_{0.5}\text{O}_3$ collected ex situ at different points along the load curve on charge and discharge. Considering first the XAS spectra. For Li_2RuO_3 , on initial charge to the beginning of the plateau, there is a pronounced increase in intensity at the leading edge of the pre-edge (lowest energy peak between 529 and 530 eV) indicating the formation of electron hole states in hybridised Ru–O orbitals consistent with Ru oxidation from +4 to +5, as previously reported^{17,25}. Across the plateau there is no further increase in this region but instead new states appear at 531 eV. After discharge, both of these changes are reversed, and the pre-

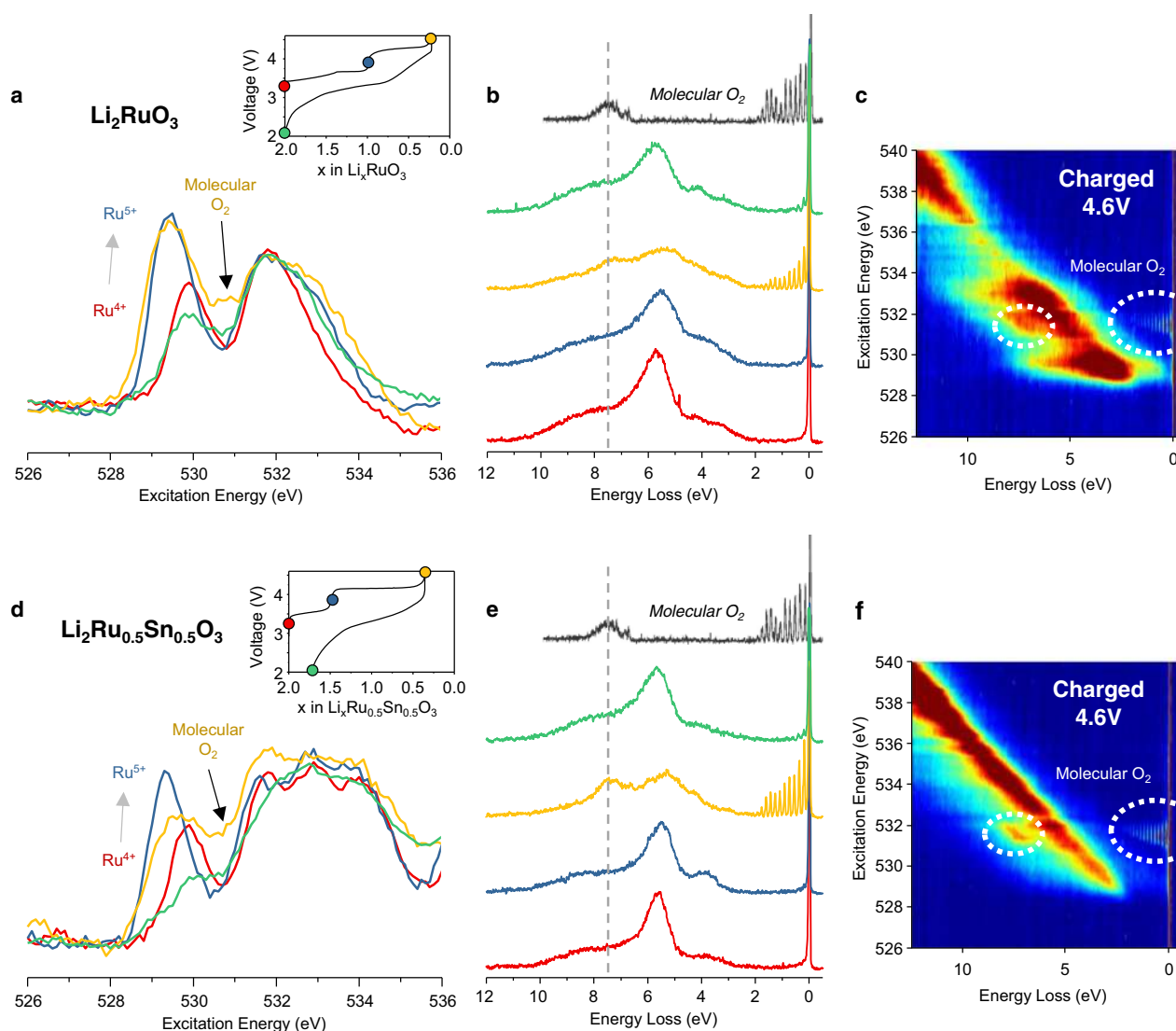


Fig. 2 O XAS and RIXS spectroscopy for Li-rich ruthenates. **a, d** O K-edge XAS spectra collected in bulk sensitive partial fluorescence yield (PFY) mode. Inset figure—load curve showing with coloured dots where on the load curve the spectra were collected. **b, e** high resolution RIXS line scans at an excitation energy of 531 eV. Spectrum of molecular O_2 gas shown for reference in black (reproduced from ref. ³⁵). The RIXS line scans reveal the formation of molecular O_2 which is reduced to O^{2-} on discharge. **c, f** High resolution RIXS maps of the O K-edge pre-edge for cathodes charged to the end of the high voltage plateau. Across the plateau there is an increase in area at 531 eV for both Li_2RuO_3 and $\text{Li}_2\text{Ru}_{0.5}\text{Sn}_{0.5}\text{O}_3$. The RIXS maps show that there are no other O–O vibrations.

edge reduces in intensity. The pre-edge for the discharged sample is comparatively broad when compared directly with that of the pristine indicating a rehybridization of the Ru–O bonding between the two samples. The structure has been shown to undergo TM migration during the first cycle and the XAS peak broadening we observe here is consistent with an increase in the local disorder around O. For $\text{Li}_2\text{Ru}_{0.5}\text{Sn}_{0.5}\text{O}_3$, the pre-edge broadening after the plateau on charge and in the discharged material is more pronounced than Li_2RuO_3 in line with the greater degree of O-redox and more extensive TM migration for the Sn-substituted material¹⁷.

To interrogate the electronic states formed at 531 eV further, RIXS measurements were performed for each sample at this excitation energy. The emission spectra are plotted as is convention, as energy loss (difference between excitation and emission energy). At the top of charge two new energy loss features become evident, a broad peak at 8 eV and a progression of sharp peaks between 0 and 2 eV, as we observed previously for $\text{Li}_{1.2}\text{Ni}_{0.13}\text{Co}_{0.13}\text{Mn}_{0.54}\text{O}_2$ and $\text{Na}_{0.75}\text{Li}_{0.25}\text{Mn}_{0.75}\text{O}_2$ ^{15,16}.

The progression of peaks in the 0–2 eV region correspond to the vibrations of a molecular O_2 diatomic, also shown in Fig. 2³⁵. The emission spectra for a range of excitation energies across the O K-edge for the fully charged electrodes were also measured and are presented as RIXS maps. The data show no evidence of any other vibrational features at different excitation energies. After discharge, these new features are much diminished in intensity indicating reversible electrochemical reduction of molecular O_2 has occurred.

The same measurements were also performed for the iridate samples and are presented in Fig. 3. $\text{Li}_2\text{Ir}_{0.5}\text{Sn}_{0.5}\text{O}_3$ exhibits very similar changes to those described for Li_2RuO_3 and $\text{Li}_2\text{Ru}_{0.5}\text{Sn}_{0.5}\text{O}_3$ consistent with the voltage profile observed. On the other hand, the RIXS spectra for Li_2IrO_3 do not show any evidence for the presence of molecular O_2 in the fully charged electrodes. Instead, a strong increase in intensity at the leading edge of the pre-edge is seen when charging Ir beyond the +5 oxidation state. This observation supports the conclusion that the high voltage plateau in Li_2IrO_3 is associated with Ir rather than O oxidation²⁶. Notably, the XAS

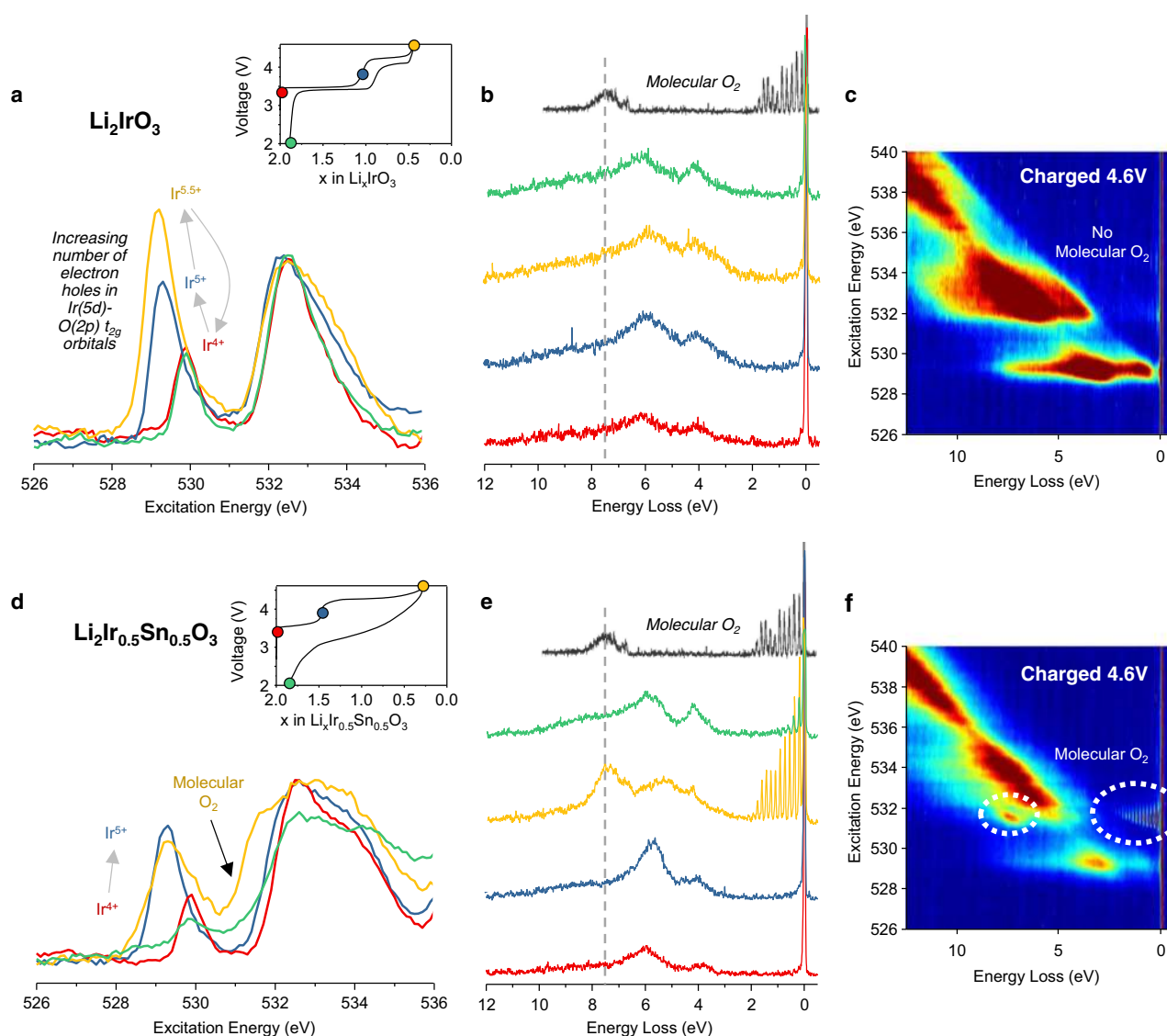


Fig. 3 O K-edge XAS and RIXS spectroscopy of Li-rich iridates. **a, d** O K-edge XAS spectra collected in bulk sensitive partial fluorescence yield (PFY) mode. Inset figure—load curve showing with coloured dots where on the load curve the spectra were collected. **b, e** High resolution RIXS line scans at an excitation energy of 531 eV. Spectrum of molecular O_2 gas shown for reference in black (reproduced from ref. 35). The RIXS line scans reveal the formation of molecular O_2 in $\text{Li}_2\text{Ir}_{0.5}\text{Sn}_{0.5}\text{O}_3$ which is reduced to O^{2-} on discharge but not in Li_2IrO_3 . **c, f** High resolution RIXS maps of the O K-edge pre-edge for cathodes charged to the end of the high voltage plateau. The RIXS maps show that there are no other vibrations.

spectra for the pristine and discharged electrodes are almost fully superimposable indicating minimal irreversible change to the electronic structure and thus structural stability.

Since the measurements are performed under ultra-high vacuum (UHV) conditions and the samples had been pumped down overnight under UHV, the electrodes will be fully out-gassed, so any molecular species that are detected are trapped within the bulk of the primary particles. To rule out the possible influence of beam damage inducing molecular O₂, we performed all our measurements at low temperature, 20 K, and conducted measurements at the same sample location over a range of timescales. The data presented in Supplementary Fig. 4 show no change in the peak spacing between spectra acquired after 30 s and 1800 s exposure times and only a minor decrease in intensity, which is in line with our previous beam sensitivity studies for molecular O₂ in Li_{1.2}Ni_{0.13}Co_{0.13}Mn_{0.54}O₂¹⁵. In that paper, we also extensively examined the effect of temperature and photon flux and showed that neither of these factors have a detectable influence on the vibrational peak spacing, reinforcing that the O₂ observed by RIXS is intrinsic to the cathode.

Although the spectroscopic data show no evidence of O species other than O₂, RIXS data were also collected for KO₂ and Li₂O₂ to rule out the possibility of O₂^{•-} and O₂²⁻. The results are presented in Fig. 4 where they are compared directly with the spectra for the Ru and Ir compounds. The peak spacing for Li₂O₂ around the elastic peak corresponding to the vibrational spectrum is almost exactly half of the peak spacing observed for molecular O₂ in the cathodes as clearly seen in the Birge-Sponer plot, Fig. 4b. This is closely in line with the vibrational frequency for O₂²⁻ which is well known to be half that of molecular O₂. For KO₂, containing the superoxide moiety O₂^{•-} of intermediate bond order to O₂ and O₂²⁻, the peak spacing lies halfway between the two. While some differences in the RIXS spectra for different peroxide and superoxide compounds is possible, the vibrational spectra associated with the elastic peak is determined primarily by the O–O bond length/strength and therefore is characteristic of these species in general. The clear distinction that can be made between O₂, O₂^{•-} and O₂²⁻ dimers demonstrates the power of high resolution RIXS and provides evidence for the formation of molecular O₂ in the Li-rich cathodes.

Discussion

Studies using X-ray photoelectron spectroscopy (XPS), electron paramagnetic resonance (EPR) and density functional theory (DFT) pointed to the possibility of peroxy-like O₂ⁿ⁻ species, where n = 1, 2 or 3^{17,20,25,36}. Scanning transmission spectroscopy (STEM) and neutron powder diffraction studies of Li₂IrO₃, suggested longer peroxy-like dimers (3 < n < 3.3)¹⁹. However, excellent though these studies are, it is a challenge for these techniques to identify unambiguously the nature of the oxidised oxygen species. XPS, being an electron emission technique, is, in general, more limited in its ability to measure bulk species than RIXS, which utilises photon emissions, and XPS can often be strongly influenced by surface contributions. Turning to local structural probes, imaging individual O–O defects in the bulk is beyond the capabilities of current STEM techniques and resolving O–O species at such low interatomic separations and concentrations is very challenging for total scattering data. Since they are magnetically complex materials, the 4d and 5d systems defy clear characterisation of oxidised O by either ¹⁷O NMR or SQUID. In contrast, the high resolution RIXS that we employ in this study is element specific, probes 50–100 nm deep into the particles, and has allowed us to clearly identify molecular O₂ in the bulk of solid materials. High resolution RIXS has already provided evidence that O²⁻ oxidation in 3d TM oxides forms molecular O₂ trapped in voids in the bulk particles. This observation is further supported by ¹⁷O NMR which not only identifies trapped molecular O₂ as the O–O species formed on charge, but also shows that it is present in quantities commensurate with that expected from the charged passed in Li_{1.2}Ni_{0.13}Co_{0.13}Mn_{0.54}O₂¹⁵.

Our RIXS and XAS results indicate that the O-redox process can be described as molecular O₂ formation throughout the cathode, both as evolved O₂ at the surface, which has already been demonstrated with operando mass spec^{19,29}, and trapped O₂ within the bulk. The 4 and 5d transition metal oxides generally exhibit greater covalency in the TM–O bond than those of their 3d counterparts; associated with the greater TMd–O2p overlap and lower electron repulsion of the larger 4 and 5d orbitals. The results presented here indicate that these more covalent systems bear closer resemblance to the 3d Li-rich materials than previously thought and that any greater covalency in the TM–O

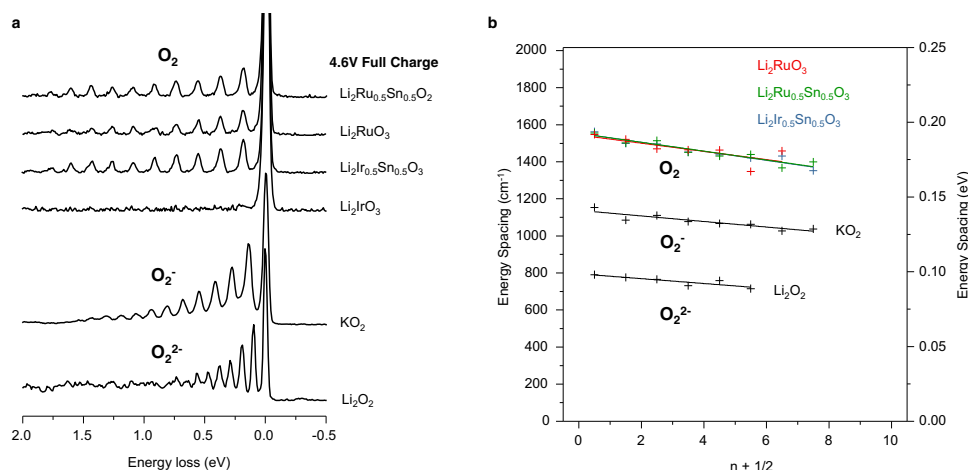


Fig. 4 Direct spectroscopic evidence against peroxides in charged 4d and 5d cathodes. **a** High resolution RIXS scans at 531 eV excitation energy for charged cathode samples and a Li₂O₂ reference collected under identical measurement conditions. KO₂ RIXS was collected at 529.6 eV, where O₂^{•-} vibrations are strongest. Peak spacing consistent with molecular O₂ is seen in the case of all cathodes except Li₂IrO₃ which is not O-redox active. There is no evidence of O₂²⁻ or O₂^{•-} vibrations in any of the cathode samples ruling out the presence of peroxides and superoxides. **b** Birge-Sponer plot showing linearly decreasing dependence of peak spacing with vibrational quantum number, *n*, consistent with the anharmonic oscillations of diatomic molecules.

bond for 4d and 5d compounds does not suppress molecular O₂ formation in favour of other O–O species.

In a recent study, Hong et al. presented Ir L₃ XANES data that showed Ir is able to oxidise beyond +5 to +5.5 in Li₂IrO₃ and Li₂Ir_{0.5}Sn_{0.5}O₃ before O-redox activity²⁶. In this regime, both materials can cycle reversibly. For Li₂Ir_{0.5}Sn_{0.5}O₃, charging can be continued beyond +5.5 consequently incurring O oxidation, TM migration, peroxide (O₂²⁻) formation and voltage hysteresis. Our results show an absence of any oxidised oxygen species in Li₂IrO₃ in accord with the Ir L₃ XANES data presented by Hong et al.²⁶. However, for Li₂Ir_{0.5}Sn_{0.5}O₃ the high resolution RIXS shows the presence of molecular O₂, rather than peroxide, as the only form of oxidised oxygen species. High resolution RIXS also reveals molecular O₂ is present in the ruthenates in contrast to previous reports of peroxides. The ability of RIXS to show an absence of signal for materials supported exclusively by TM-redox and identify oxidised O when it is present in O-redox materials demonstrates its utility for probing oxidised O species. Ir⁵⁺, low spin t_{2g}⁴, has 1 more electron than Ru⁵⁺, t_{2g}³, and it is spin-paired, Fig. 5a. Removal of this higher energy spin down electron occurs at a lower voltage than for an electron on Ru⁵⁺. The oxidation of O²⁻ sits between the energies for Ir^{5+/6+} and Ru^{5+/6+} such that Ir⁵⁺ is oxidised before O²⁻ (i.e. at a lower voltage) whereas Ru⁵⁺

is not. The voltages of the redox couples derived from dQ/dV analysis of the electrochemical load curves in Fig. 1 are shown in Fig. 5b. The substitution of Ir for Sn limits the Ir redox capacity increasing the amount of extractable Li available to be charge compensated by O-redox explaining why substantial O oxidation is observed for Li₂Ir_{0.5}Sn_{0.5}O₃.

Much like the 3d TM Li-rich O-redox systems, those based on 4d and 5d TM elements exhibit TM migration, loss of honeycomb ordering, O-loss and voltage hysteresis. The vibrational spectra measured by RIXS now also show that molecular O₂, rather than peroxides or peroxy-like species, are formed in all of these systems indicating TM–O covalency has limited effect on the bond order of the O–O dimer in the bulk of the cathodes. Future research efforts on Li-rich cathodes should focus on chemical and structural modifications other than covalency of the host network to improve their performance.

Methods

Materials preparation. Li₂RuO₃ and Li₂Ru_{0.5}Sn_{0.5}O₃ were synthesised from RuO₂ (99.9% Alfa Aesar), SnC₂O₄ (98% Alfa Aesar) and Li₂CO₃ (99+% Merck) mixed in the appropriate ratios with 10% excess Li₂CO₃. Calcination was performed in air at 800 °C for 6 h, 900 °C for 12 h and then 1100 °C for 12 h with intermediate grinding. Li₂IrO₃ and Li₂Ir_{0.5}Sn_{0.5}O₃ were synthesised from IrO₂ (99.9% Alfa Aesar), SnO₂ (99.9% Alfa Aesar) and Li₂CO₃ (99+% Merck) mixed in the appropriate ratios with 10% excess Li₂CO₃. Calcination was performed in air at 1000 °C for 12 h and 900 °C for 36 h with intermediate grinding. The as-prepared materials were transferred to an Ar-filled glovebox and handled under inert atmosphere for all further manipulations. Li₂O₂ (95%, ACROS Organics) and KO₂ (Sigma Aldrich) standards were used as supplied.

Electrochemistry. Self-supporting electrode films were prepared by grinding the as-synthesised materials with acetylene black and polytetrafluoroethylene in a 8:1:1 mass ratio in a pestle and mortar and subsequently calendared. Electrochemical cycling was performed in coin cells with LP30 electrolyte and a lithium metal foil counter electrode. Cells were disassembled at different states of charge and the electrodes rinsed with dry dimethylcarbonate for ex situ analysis.

Powder X-ray diffraction. Powder X-ray diffraction patterns were obtained for the as-prepared materials using a Cu source Rigaku SmartLab diffractometer equipped with a Ge(220) double bounce monochromator and without exposure to air. Reitveld profile refinements were performed using the GSAS suite of programs.

X-ray absorption spectroscopy and resonant inelastic X-ray scattering. X-ray absorption spectroscopy and resonant inelastic X-ray scattering data were obtained at the I21 beamline, Diamond Light Source. Samples were transferred to the spectrometer using a vacuum transfer suitcase to avoid air exposure and were pumped down to UHV and left to fully degas overnight. O K-edge spectra were obtained in partial fluorescence mode for bulk sensitivity. RIXS line scans were recorded at five different sample locations and averaged together. RIXS maps were collected at 0.2 eV intervals in excitation energy. All measurements were performed at 20 K to minimise any possible beam damage.

Data availability

Supporting research data has been deposited in the Oxford Research Archive and is available under this DOI: 10.5287/oxfordia:eyyG8ovA0.

Received: 29 September 2020; Accepted: 8 April 2021;

Published online: 20 May 2021

References

- Koga, H. et al. Different oxygen redox participation for bulk and surface: a possible global explanation for the cycling mechanism of Li_{1.20}Mn_{0.54}Co_{0.13}Ni_{0.13}O₂. *J. Power Sources* **236**, 250–258 (2013).
- Seo, D.-H. et al. The structural and chemical origin of the oxygen redox activity in layered and cation-disordered Li-excess cathode materials. *Nature Chemistry* **8**, 692–697 (2016).
- Muhammad, S. et al. Evidence of reversible oxygen participation in anomalously high capacity Li- and Mn-rich cathodes for Li-ion batteries. *Nano Energy* **21**, 172–184 (2016).
- Lu, Z. & Dahn, J. R. Understanding the anomalous capacity of Li/Li[Ni_xLi_(1/3-2x/3)Mn_(2/3-x/3)]O₂ cells using in situ X-Ray diffraction and electrochemical studies. *J. Electrochem. Soc.* **149**, A815–A815 (2002).

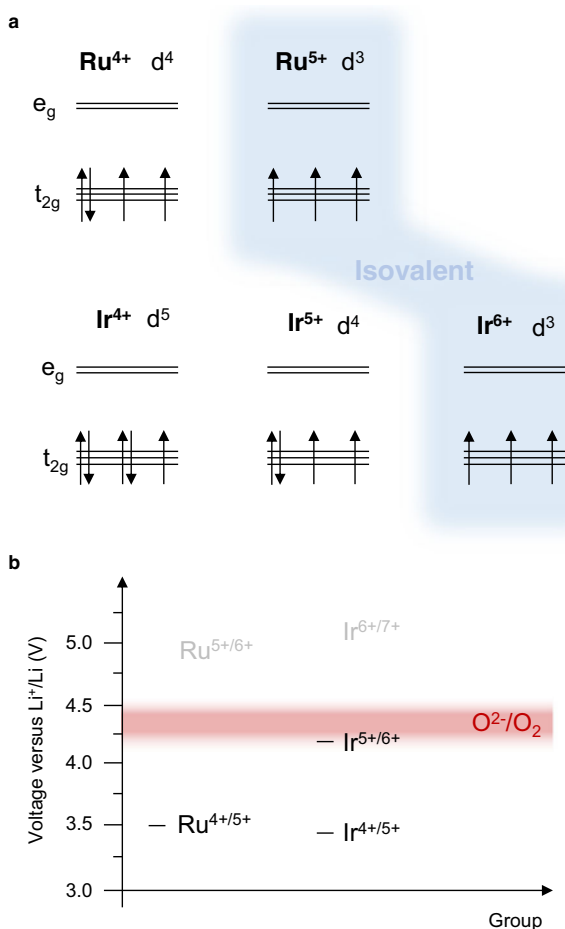


Fig. 5 Redox potentials. **a** d electron configurations for different oxidation states of Ru and Ir. The spin down electron on Ir⁵⁺ is at a higher energy and hence oxidised at a lower voltage than removal of a spin up electron from the stable d³ configuration of Ru⁵⁺. Since oxidation of Ir⁵⁺ occurs before O²⁻/O₂ and Ru⁵⁺ does not, we place O²⁻/O₂ between the two redox couples in the figure (**b**). The values of the redox couples shown in black in (**b**) were obtained from dQ/dV analysis extracted from the data in Fig. 1.

- Johnson, C. S. et al. The significance of the Li_2MnO_3 component in 'composite' $x\text{Li}_2\text{MnO}_3 \cdot (1-x)\text{LiMn}_{0.5}\text{Ni}_{0.5}\text{O}_2$ electrodes. *Electrochem. Commun.* **6**, 1085–1091 (2004).
- Koga, H. et al. Reversible oxygen participation to the redox processes revealed for $\text{Li}_{1.20}\text{Mn}_{0.54}\text{Co}_{0.13}\text{Ni}_{0.13}\text{O}_2$. *J. Electrochem. Soc.* **160**, A786–A792 (2013).
- Lu, Z., Beaulieu, L. Y., Donaberg, R. A., Thomas, C. L. & Dahn, J. R. Synthesis, structure, and electrochemical behavior of $\text{Li}[\text{Ni}_x\text{Li}_{1/3-2x/3}\text{Mn}_{2/3-x/3}]\text{O}_2$. *J. Electrochem. Soc.* **149**, A778–A778 (2002).
- Assat, G. et al. Direct quantification of anionic redox over long cycling of Li-Rich NMC via hard X-ray photoemission spectroscopy. *ACS Energy Lett.* **3**, 2 (2018).
- Luo, K. et al. Charge-compensation in 3d-transition-metal-oxide intercalation cathodes through the generation of localized electron holes on oxygen. *Nat. Chem.* **8**, 684–691 (2016).
- Gent, W. E. et al. Coupling between oxygen redox and cation migration explains unusual electrochemistry in lithium-rich layered oxides. *Nat. Commun.* **8**, 2091 (2017).
- Tran, N. et al. Mechanisms associated with the "Plateau" observed at high voltage for the overlithiated $\text{Li}_{1.12}(\text{Ni}_{0.425}\text{Mn}_{0.425}\text{Co}_{0.15})_{0.88}\text{O}_2$ System. *Chem. Mater.* **20**, 4815–4825 (2008).
- Armstrong, A. R. et al. Demonstrating oxygen loss and associated structural reorganization in the lithium battery cathode $\text{Li}[\text{Ni}_{0.2}\text{Li}_{0.2}\text{Mn}_{0.6}]\text{O}_2$. *J. Am. Chem. Soc.* **128**, 8694–8698 (2006).
- Croy, J. R., Balasubramanian, M., Gallagher, K. G. & Burrell, A. K. Review of the U.S. Department of Energy's "deep Dive" Effort to Understand Voltage Fade in Li- and Mn-Rich Cathodes. *Acc. Chem. Res.* **48**, 2813–2821 (2015).
- Chen, H. & Islam, M. S. Lithium Extraction Mechanism in Li-Rich Li_2MnO_3 involving oxygen hole formation and dimerization. *Chem. Mater.* **28**, 6656–6663 (2016).
- House, R. A. et al. First-cycle voltage hysteresis in Li-rich 3d cathodes associated with molecular O_2 trapped in the bulk. *Nature Energy* **5**, 777–785 (2020).
- House, R. A. et al. Superstructure control of first-cycle voltage hysteresis in oxygen-redox cathodes. *Nature* **577**, 502–508 (2020).
- Sathiyar, M. et al. Reversible anionic redox chemistry in high-capacity layered-oxide electrodes. *Nat. Mater.* **12**, 827–835 (2013).
- Sathiyar, M. et al. High Performance $\text{Li}_2\text{Ru}_{1-y}\text{Mn}_y\text{O}_3$ ($0.2 \leq y \leq 0.8$) cathode materials for rechargeable lithium-ion batteries: their understanding. *Chem. Mater.* **25**, 1121–1131 (2013).
- McCalla, E. et al. Visualization of O-O peroxo-like dimers in high-capacity layered oxides for Li-ion batteries. *Science* **350**, 1516–1521 (2015).
- Saubanère, M., McCalla, E., Tarascon, J.-M. & Doublet, M.-L. The intriguing question of anionic redox in high-energy density cathodes for Li-ion batteries. *Energy Environ. Sci.* **9**, 984–991 (2016).
- Perez, A. J. et al. Strong oxygen participation in the redox governing the structural and electrochemical properties of Na-rich layered oxide Na_2IrO_3 . *Chem. Mater.* **28**, 8278–8288 (2016).
- Rozier, P. et al. Anionic redox chemistry in Na-rich $\text{Na}_2\text{Ru}_{1-y}\text{Sn}_y\text{O}_3$ positive electrode material for Na-ion batteries. *Electrochem. Commun.* **53**, 29–32 (2015).
- ben Yahia, M., Vergnet, J., Saubanère, M. & Doublet, M.-L. Unified picture of anionic redox in Li/Na-ion batteries. *Nat. Mater.* **18**, 496–502 (2019).
- Xie, Y., Saubanère, M. & Doublet, M.-L. Requirements for reversible extra-capacity in Li-rich layered oxides for Li-ion batteries. *Energy Environ. Sci.* **10**, 266–274 (2017).
- Sathiyar, M. et al. Electron paramagnetic resonance imaging for real-time monitoring of Li-ion batteries. *Nat. Commun.* **6**, 6276 (2015).
- Hong, J. et al. Metal-oxygen decoordination stabilizes anion redox in Li-rich oxides. *Nat. Mater.* **18**, 256–265 (2019).
- Mortemard de Boisse, B. et al. Intermediate honeycomb ordering to trigger oxygen redox chemistry in layered battery electrode. *Nat. Commun.* **7**, 11397 (2016).
- Mortemard de Boisse, B. et al. Coulombic self-ordering upon charging a large-capacity layered cathode material for rechargeable batteries. *Nat. Commun.* **10**, 1–7 (2019).
- Yu, Y. et al. Revealing electronic signatures of lattice oxygen redox in lithium rhenates and implications for high-energy Li-ion battery material designs. *Chem. Mater.* **31**, 7864–7876 (2019).
- Kobayashi, H., Tabuchi, M., Shikano, M., Kageyama, H. & Kanno, R. Structure, and magnetic and electrochemical properties of layered oxides, Li_2IrO_3 . *J. Mater. Chem.* **13**, 957–962 (2003).
- Li, L. et al. Probing electrochemically induced structural evolution and oxygen redox reactions in layered lithium iridate. *Chem. Mater.* **31**, 4341–4352 (2019).
- Charles, N. et al. Toward establishing electronic and phononic signatures of reversible lattice oxygen oxidation in lithium transition metal oxides for Li-ion batteries. *Chem. Mater.* **32**, 5502–5514 (2020).
- Rouxel, J. Anion–cation redox competition and the formation of new compounds in highly covalent systems. *Chem. - A Eur. J.* **2**, 1053–1059 (1996).
- Sharpe, R. et al. Redox chemistry and the role of trapped molecular O_2 in Li-rich disordered rocksalt oxyfluoride cathodes. *J. Am. Chem. Soc.* **142**, 21799–21809 (2020).
- Arhammar, C. et al. Unveiling the complex electronic structure of amorphous metal oxides. *Proc. Natl Acad. Sci. USA* **108**, 6355–6360 (2011).
- Foix, D., Sathiyar, M., McCalla, E., Tarascon, J.-M. & Gonbeau, D. X-ray photoemission spectroscopy study of cationic and anionic redox processes in high-capacity Li-ion battery layered-oxide electrodes. *J. Phys. Chem. C* **120**, 862–874 (2016).

Acknowledgements

P.G.B. is indebted to the EPSRC, including the SUPERGEN programme (EP/L019469/1), the Henry Royce Institute for Advanced Materials (EP/R00661X/1, EP/S019367/1, EP/R010145/1, EP/L019469/1) and the Faraday Institution (FIRG007, FIRG008) for financial support. We acknowledge Diamond Light Source for time on I21 under proposal MM25589-1.

Author contributions

R.A.H. conceived and conducted the experimental work. R.A.H., J.J.M. and J.P. working closely with K.-J. Z. and team S.A., A.N., M.G.F. conducted, processed and interpreted the RIXS and soft XAS measurements. G.J.R. assisted collecting supporting data. R.A.H. and P.G.B. wrote the manuscript with contributions from all authors.

Competing interests

The authors declare no competing interests.

Additional information

Supplementary information The online version contains supplementary material available at <https://doi.org/10.1038/s41467-021-23154-4>.

Correspondence and requests for materials should be addressed to P.G.B.

Peer review information *Nature Communications* thanks the anonymous reviewers for their contribution to the peer review of this work.

Reprints and permission information is available at <http://www.nature.com/reprints>

Publisher's note Springer Nature remains neutral with regard to jurisdictional claims in published maps and institutional affiliations.



Open Access This article is licensed under a Creative Commons Attribution 4.0 International License, which permits use, sharing, adaptation, distribution and reproduction in any medium or format, as long as you give appropriate credit to the original author(s) and the source, provide a link to the Creative Commons license, and indicate if changes were made. The images or other third party material in this article are included in the article's Creative Commons license, unless indicated otherwise in a credit line to the material. If material is not included in the article's Creative Commons license and your intended use is not permitted by statutory regulation or exceeds the permitted use, you will need to obtain permission directly from the copyright holder. To view a copy of this license, visit <http://creativecommons.org/licenses/by/4.0/>.

© The Author(s) 2021